Ultra-efficient Copper Ions Adsorption of Chitosan-montmorillonite Composite Aerogel for Wastewater Treatment

Xin Ye
Nanjing Tech University
Sisi Shang
Nanjing Tech University
Yifan Zhao
Nanjing Tech University
Sheng Cui (cui2002sheng@126.com)
Nanjing University of Technology
Ya Zhong
Nanjing Tech University
Longjin Huang
Nanjing Tech University

Research Article

Keywords: Chitosan, Montmorillonite, Cu2+, Aerogel, Environmental protection

Posted Date: March 1st, 2021

DOI: https://doi.org/10.21203/rs.3.rs-242683/v1

Ultra-efficient copper ions adsorption of Chitosan-montmorillonite composite aerogel for wastewater treatment

Xin Ye[1,2], Sisi Shang[1,2],Yifan Zhao[1,2],Sheng Cui[1,2*],Ya Zhong[1,2*],Longjin Huang[1,2]

1 College of Materials Science and Engineering, Nanjing Tech University, 211800 Nanjing, China

2 Jiangsu Collaborative Innovation Center for Advanced Inorganic Function Composites, Nanjing Tech University, 211800 Nanjing, China

***Corresponding Author**

Sheng Cui

E-mail address: *cui2002sheng@126.com*

Ya Zhong

E-mail address: *yzhong@njtech.edu.cn*

Abstract

The modified montmorillonite(MMT) has a two-dimensional stable and ordered lamellar structure. The addition of chitosan(CS) cross-links the two-dimensional sheets to build a three-dimensional network structure with a high specific surface area. We have prepared the best MMT-based water treatment materials that have been reported. This new type of aerogel can efficiently adsorb heavy metal ions in wastewater. The structure and performance of the composite material were characterized in this article. Besides, the adsorption kinetics, adsorption thermodynamics, pH influence, and recycling performance are all focused on. The adsorption equilibrium time of CS-MMT2 is 50 min. The removal rate of Cu^{2+} is as high as 98.21%. The maximum adsorption capacity is 86.95 mg/g. The adsorption process of Cu^{2+} by CS-MMT composite aerogel conforms to the

quasi-second-order kinetic model and the Langrangian adsorption isotherm. After three cycles, the removal rate of Cu^{2+} by CS-MMT2 remained above 80%. This article also involves the discussion of the material's adsorption mechanism for Cu^{2+}. This is a kind of environmentally friendly material that can be mass-produced, cheap, efficient, and excellent, which is of great significance to the development of environmental protection.

Key Words: Chitosan, Montmorillonite, Cu^{2+}, Aerogel, Environmental protection

0.Introduction

With the exploitation of natural resources, the pollution of water resources has attracted much attention(Kolpin et al. 2002). In several countries and regions, it has already exceeded the self-purification capacity of natural water bodies, causing much severe environmental pollution(Fu and Wang 2011). Heavy metal pollution is one of the most important parts of the water environment pollution(Jarup 2003; Zou et al. 2016). In industry and agriculture, a large number of pollutants, including heavy metals, have been discharged into rivers, which resulted in deteriorating water quality, causing a series of serious consequences(Bailey et al. 1999).

Copper is an essential trace element in the human body. It can be absorbed from various sources, such as food, dust, and water. Excess copper may lead to several symptoms such as nausea, vomiting, abdominal muscle pain. Accumulating in the liver, it may cause various diseases such as gastrointestinal discomfort, kidney, and liver damage (Thit et al. 2020). It can be fatal at extreme doses (Shabbir et al. 2020). Therefore, it is essential to remove residual copper ions in water. Numerous articles have reported various sewage treatment methods containing heavy metal ions, including adsorption, ion exchange, chemical precipitation, membrane filtration, electrochemical

techniques, and reverse osmosis (Moja et al. 2020). Compared with others, adsorption is a simple, easy-to-operate, and inexpensive way to treat heavy metal ions (El-Kousy et al. 2020). Recent research has focused on relatively low-cost adsorbents such as zeolite(Bailey et al. 1999), montmorillonite(Uddin 2017), kaolinite clay(Yuan et al. 2015), mineral silicate(Luo et al. 2010), sepiolite(Sun et al. 2013), chitosan polymer(Wan et al. 2010), and biological packing(Wu et al. 2004), etc. For any adsorbent, the adsorption capacity is the most critical technical indicator. Especially for low-concentration heavy metal ion wastewater, the development of nano-adsorption materials has a long way to go(Liu et al. 2020b). Therefore, it is necessary to obtain a new adsorbent with high adsorption capacity, high specific surface area, rich pore structure, abundant sources, low cost, good stability, easy recovery, and regeneration.

In recent years, aerogel has been considered a promising insulation material. (Baetens et al. 2011) At the same time, high porosity and large specific surface area show superior adsorption capacity (Cui et al. 2018). It can be widely used in sewage treatment, air purification, nuclear waste treatment, and other environmental protection fields(Pierre and Pajonk 2002).

Modified clay, such as montmorillonite, is regarded as one of the best inorganic adsorbents because of its high utilization rate, friendly environment, and high negative charge, which can absorb positively charged metal ions(Mahouachi et al. 2020). Chitosan is hydrophilic, biocompatible, biodegradable, non-toxic, has high mechanical strength and film-forming properties, as well as antibacterial properties(Li et al. 2016). The amino ($-NH_2$) and hydroxyl (-OH) groups inherent in the chemical structure of chitosan are the main functional groups that adsorb various heavy metals in water. By modifying the structure of chitosan with -COOH group, its solubility at pH=7 can be increased without affecting the above properties(Wang et al. 2017). Studies have

shown that ionic imprinted montmorillonite nanosheet/chitosan (IIMNC) gel beads provide active adsorption sites through their highly efficient cation exchange performance for the selective adsorption of Cu^{2+}(Qin et al. 2020). The montmorillonite-chitosan composite material can provide hydrophobicity and functional groups to improve the performance of montmorillonite in wastewater treatment(Hu et al. 2017b). The interaction sequence of adsorption-related groups in the chitosan-Montmorillonite composite showed that the adsorption capacity of bonding with NH_3^+ may be greater than that of bonding with hydroxyl(Hu et al. 2017a). The clay-chitosan nanocomposite material is expected to achieve a major breakthrough in the treatment of heavy metal ion wastewater.

Our team combined chitosan aerogel and montmorillonite designed a new high-efficiency adsorbent. Montmorillonite can be used as ideal templates for preparing nanomaterials and supporting chitosan hydrogels due to their high surface area and stable structure. We use the LiOH/urea dissolving system to process chitosan raw materials and the chemical precipitation method to compound Montmorillonite. By adjusting the concentration of the initial reactants, the size, pore size, and mechanical properties of the synthesized CS-MMT aerogel can be determined. CS-MMT aerogel nanocomposite can be used as an environmentally friendly adsorbent for the removal of Cu^{2+} from wastewater. With its outstanding performance, it will occupy a place in the field of wastewater treatment. The adsorption kinetics and adsorption thermodynamics were used to systematically study the maximum adsorption capacity. The separation and reusability of CS-MMT aerogel were also studied in detail.

1.Experimental Section

1.1 Fabrication of CS-MMT aerogel

CS-MMT aerogel was prepared by sol-gel method (SI Fig. 1), which could be broken and

regenerated at low temperature(SI Section 1). According to the absorbance value of Cu^{2+} in the supernatant, the concentration, adsorption capacity, and removal efficiency of Cu^{2+} in the remaining solution were calculated using equations ((1)-(4)).

$$A = 0.0191C + 0.0124 \quad (1)$$

$$Ce = \frac{C}{V_1} \quad (2)$$

$$Qe = \left[\frac{(C_0 - C_e) \times V_2}{m_1}\right] \quad (3)$$

$$S(\%) = \frac{C_0 - C_e}{C_0} \times 100\% \quad (4)$$

Where *C* is the content of Cu^{2+} in the residual solution after adsorption, which can be calculated by different absorbance values(μg). C_0 before for adsorption of Cu^{2+} solution concentration (mg/mL). C_e for the adsorption of Cu^{2+} solution concentration (mg/mL). *m* is obtained from the standard curve of Cu^{2+} dosage (μg). m_1 as adsorbent dose (mg). V_1 for copper water volume (mL). Q_e for equilibrium adsorption Cu (II) the amount of (mg/g). V_2 to join Cu^{2+} the volume of a solution (mL), *S* for Cu^{2+} removal efficiency.

2. Results and discussion

2.1 XPS, XRD and FT-IR analysis

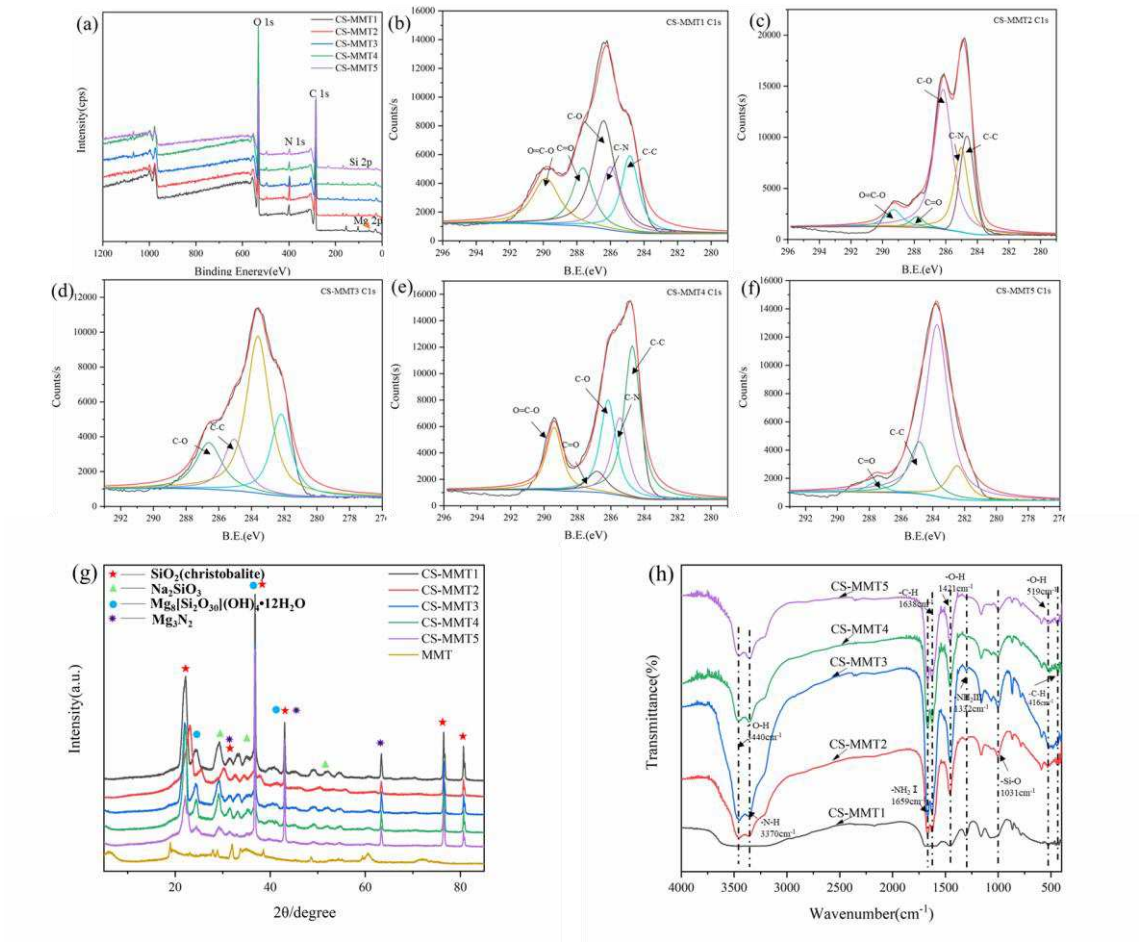

Fig. 1 (a) XPS survey spectrum, (b~f) C1s spin-orbit peaks of CS-MMTs, (g) XRD patterns of CS-MMTs and MMT, (h) FTIR spectra of CS-MMTs

To further analyze the interaction between MMT and CS matrix, X-ray photoelectron spectroscopy is used to analyze the surface chemical state of different components of CS-MMTs (Fig. 1(b~f)). The C spectrum shows that the CS-MMTs are rich in C-C, C=O, and C-O/C-N groups. The peak at 283.9 eV corresponds to the binding energy of the C-N bond, and the peaks of C=O and C-C mainly appear at about 286.8 eV and 285.0 eV. (Wu et al. 2020). Compared with other components, the C1 s of CS-MMT2 is significantly enhanced, and the intensity of the C-N peak is also significantly increased, proving that MMT was successfully modified by CS. The O1s (531.8 eV) peak is attributed to hydroxyl oxygen, indicating that siloxane was successfully converted to hydroxyl oxygen. (Guo et al. 2019). However, the N-element XPS spectrum showed a certain

116 amount of C-N and N-O in CS-MMT. Besides, peaks of Si 2p(103eV) and Mg2p (55eV)
117 corresponding to MMT were found in the spectrum of CS-MMT2(Akar et al. 2020), indicating the
118 successful combination of CS and MMT.

119 The crystal phase and phase composition of CS-MMT composite aerogel were analyzed by
120 XRD (Fig. 1 (g)). According to extensive studies, MMT is a clay mineral in the form of octahedral
121 crystals. The characteristic spikes show high crystallinity of nano-MMT at 5.9°, 19°, and 26°.
122 According to the Scherer equation, we can easily calculate that the interlayer spacing of nano-
123 montmorillonite is 1.593nm. In contrast, the XRD patterns of the chitosan-modified
124 montmorillonite composite aerogels have obvious changes, indicating that the crystal structure of
125 the composite aerogel has changed significantly. By comparing and analyzing the standard spectra,
126 we can infer that the crystal structure of CS-MMT is roughly the same as that of square quartz.
127 Besides, we can notice that there is a broad peak at 29°. As the ratio of nano-montmorillonite
128 increases, the peak intensity gradually decreases. We attribute this to the cation exchange between
129 the protonated amino groups of chitosan and the cations in the montmorillonite layer, which results
130 in such formation of disordered exfoliation structures.

131 As shown in Fig.1(h), the hydroxyl groups of amide or hydroxide combined with amino groups
132 in montmorillonite and chitosan mainly appear at about 3400 cm^{-1}, which is consistent with previous
133 reports (Liu et al. 2020a). The amide stretching of the chitosan-modified montmorillonite composite
134 appeared at about 1640 cm^{-1}. All the CS-MMT composite aerogels showed characteristic silica sharp
135 bands around 1031 cm^{-1}. The bending vibrations of Si-O-Mg and Si-O-Si appeared at 1527 cm^{-1} and
136 470 cm^{-1}, respectively(Zhu et al. 2017). There are strong peaks at 3440 cm-1 and 1659 cm-1, which
137 correspond to the overlapping stretching vibrations of hydroxyl and amino groups and the stretching

vibrations of carboxyl groups. The peak at 1332 cm^{-1} is the stretching vibration of amino. The FT-IR is a great proof of the successful preparation of CS-MMT composite aerogels.

2.2 SEM analysis

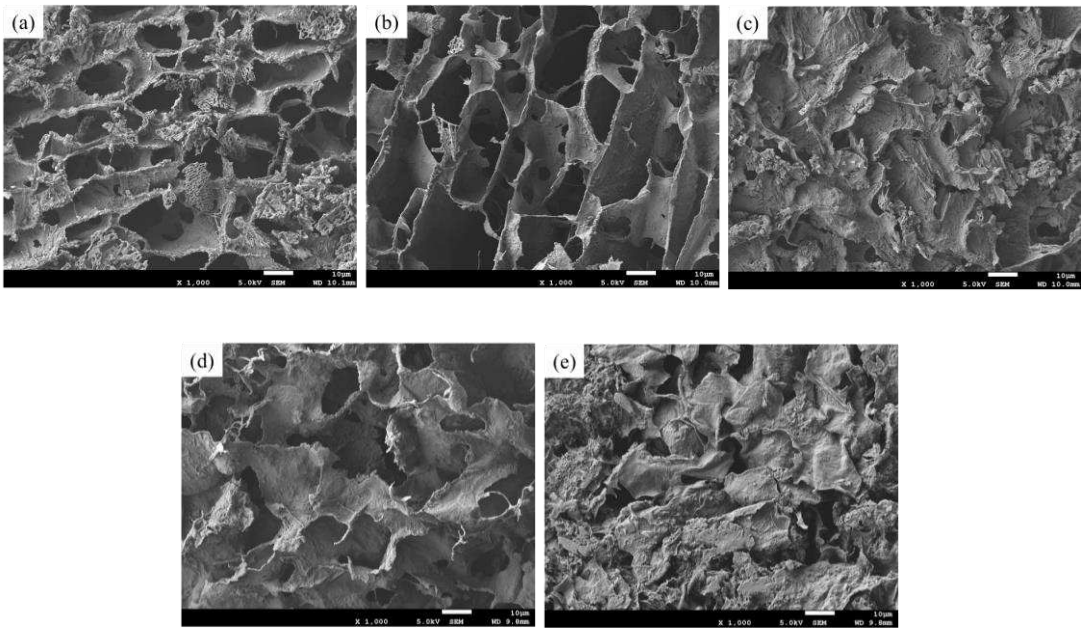

Fig. 2 SEM image of (a)CS-MMT1, (b)CS-MMT2, (c)CS-MMT3, (d)CS-MMT4, (e)CS-MMT5

As is shown in Fig. 2 , the CS-MMT composite aerogels of different components all present a clear layered structure. CS connects the montmorillonite laminates in a fiber-like cross-linking manner. As shown in Fig. 2(b), CS-MMT2 composite aerogel has a large number of thin-layer structures and a certain interlayer space. The doping of CS cross-links the layers of MMT to build a micron-level pore structure. This three-dimensional porous structure can greatly increase the specific surface area of the material, laying a solid foundation for the adsorption of heavy metal ions. The C, N, O, and Si elements of CS-MMT2 aerogel are uniformly distributed. It contains a large number of oxygen-containing functional groups, oxides, and nitrides. By TG analysis, CS-MMT showed higher degradation temperature (SI Section2, Fig. S2, and S3).

2.2 The Specific surface area and pore size analysis

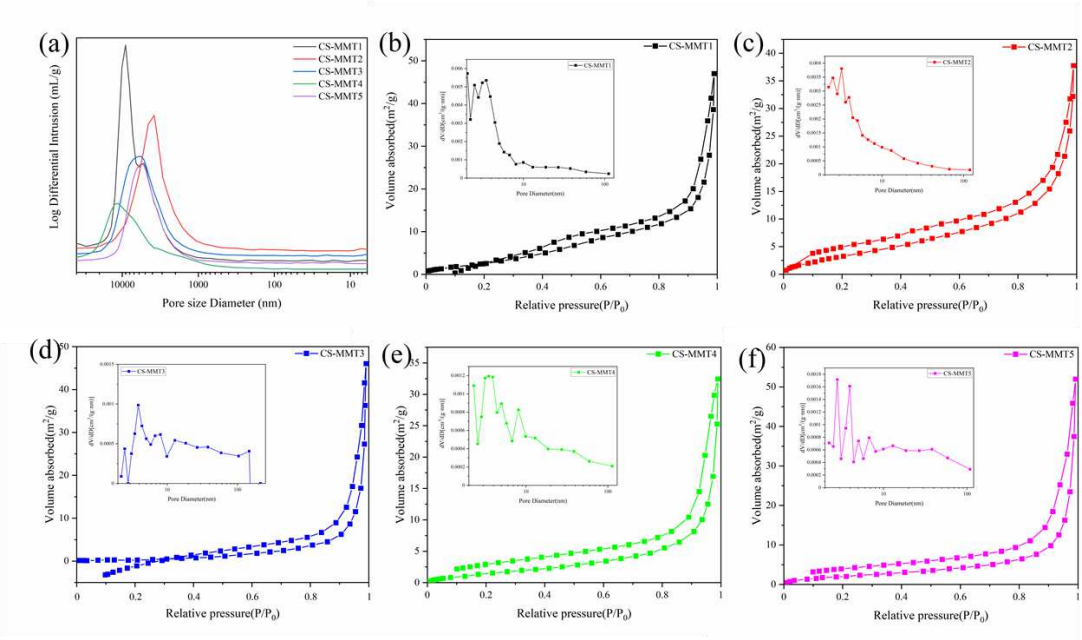

154

155 **Fig. 3** (a) Mercury intrusion test, (b~f) N_2 Adsorption–desorption isotherms and pore size

156 distributions of CS-MMT composite aerogels with different components

157 The shape of this type of hole should be a slit-like tubular capillary structure with both ends

158 open. (Zhao et al. 2020). As is shown in Fig.3(a~f), when the relative pressure P/P_0 was 0-0.6, the

159 N_2 adsorption increased slowly, which proved that there were a few micropores in the samples. In

160 this stage, nitrogen molecules are gradually adsorbed from monolayer to multilayer into the porous

161 structure. Subsequently, when the relative pressure was between 0.6-0.99, the nitrogen adsorption

162 capacity at the high-pressure end increased sharply, indicating the presence of mesopore and

163 macropore in the material. According to the physical property parameters in SI Table S1, the specific

164 surface area of CS-MMT2 is relatively high, which is 14.133m^2/g, and the pore diameter distribution

165 was uniform. Combined with SEM images(Fig.1(b)), it was found that there was a stable three-

166 dimensional network structure. (Chu et al. 2019). Because the nitrogen adsorption and desorption

167 specific surface and pore size test can be widely used in the test of porous materials with mesoporous

168 structure, it is only of reference value for macroporous materials. We conducted mercury intrusion

tests on all five CS-MMT samples. According to the analysis of mercury injection pore size, the pores are mainly mesopore and macropore. The average pore sizes of composite aerogels are 1242.89 nm(CS-MMT1), 889.29 nm(CS-MMT2), 1012.60 nm(CS-MMT3), 3942.97 nm(CS-MMT4), and 1159.19 nm(CS-MMT5). The pore size ranges from 50-100 μm. Undoubtedly, large specific surface area and porous structure provided more abundant active sites for rapid absorption of Cu^{2+}.

2.3 Structure model and adsorption mechanism

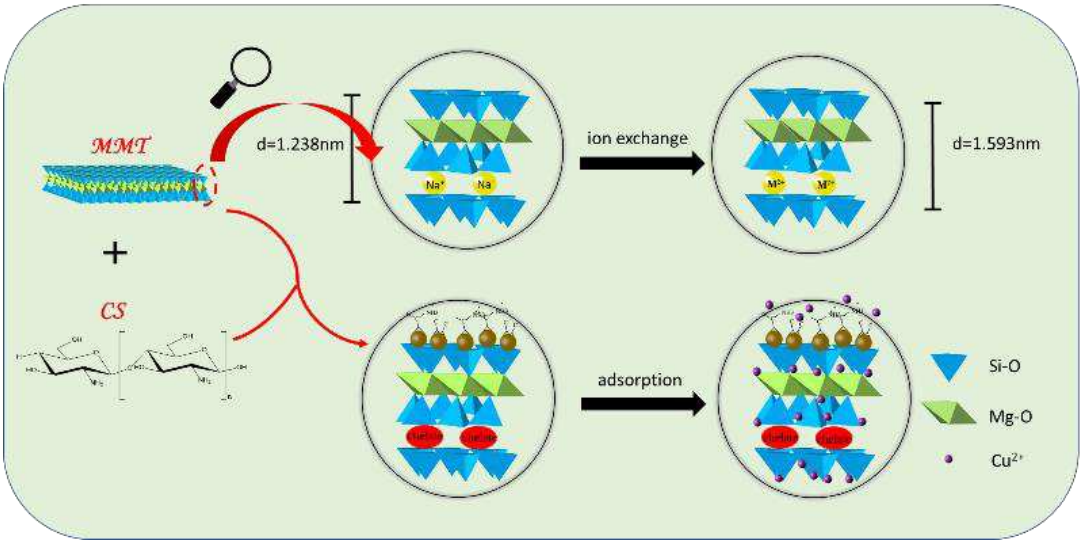

Fig. 4 Schematic diagram of structure model and adsorption mechanism

According to detailed characterization data, we can get the following material structure model (Fig. 4). The montmorillonite layer is modified by organic quaternary ammonium salt ions. Combined with the XRD diffraction pattern, it can be seen that the interlayer spacing of montmorillonite increases from 1.236 to 1.593 nm. XRD, FT-IR, and XPS are used for detailed elements and surface state analysis. We speculate that strong alkali treatment and ball milling break the Si-O and Mg-O bonds of the unit cell in montmorillonite. The amino groups of chitosan cross-link the active bonds and the -OH and amino groups carried by the surface sheet, forming such CS-

MMT composite aerogel. Cu^{2+} will not only chelate and react with the broken bonds on the surface of CS-MMT, at the same time, the pores and lamella structure of the aerogel are also positively related to the adsorption capacity.

2.4 Adsorption property of CS-MMTs towards Cu^{2+}

Adsorption equilibrium time and adsorption kinetics

CS-MMT composite aerogel adsorbed Cu^{2+} at different times (SI Section 2). The adsorption rates of the five adsorbents at different times are sorted in Fig. 5. It can be seen from the adsorption curve and adsorption efficiency that all adsorbents have a high adsorption efficiency of Cu^{2+} in the initial stage of the adsorption reaction. As time goes on, the adsorption process slows down until an adsorption equilibrium is finally reached. In the initial stage of adsorption in this experiment, the Cu^{2+} adsorption material causes concentration diffusion in the solution, and the active adsorption sites on the montmorillonite can combine with Cu^{2+} at different adsorption rates and numbers. As the concentration gradient of Cu^{2+} decreases, the adsorption behavior on the adsorbent gradually decreases, which in turn causes the adsorption rate to slow down. At the same time, as the chelation reaction progresses, the adsorption sites are gradually occupied, and the adsorption reaction reaches equilibrium. From the relationship between adsorption time and adsorption efficiency, it can be seen that the adsorption efficiency of different components of CS-MMT composite aerogel on Cu^{2+} is not significantly different under the same experimental conditions. The adsorption efficiency of CS-MMT2 can be around 99%, and the adsorption equilibrium was reached at about 50min, indicating that CS-MMT2 composite aerogel has a strong adsorption capacity for Cu^{2+}. To elucidate the adsorption kinetics of CS-MMT composite aerogel on Cu^{2+}, the quasi-first-order model (Eq5) and quasi-second-order model (Eq6) were used to fit the adsorption data of Cu^{2+} as follows:

$$\lg(Q_e - Q_t) = \lg Q_e - \frac{k_1 t}{2.303} \quad (5)$$

$$\frac{t}{Q_t} = \frac{t}{Q_e} + \frac{1}{k_2 Q_e^2} \quad (6)$$

Where Q_e is the adsorption amount when the adsorption process reaches adsorption equilibrium (mg/g), Q_t is the adsorption amount corresponding to t at a certain moment in the adsorption process (mg/g), $k_1$and k_2 are pseudo-first-order (min^{-1}) and pseudo-second-order rate constants (g/ (mg·min^{-1})), respectively.

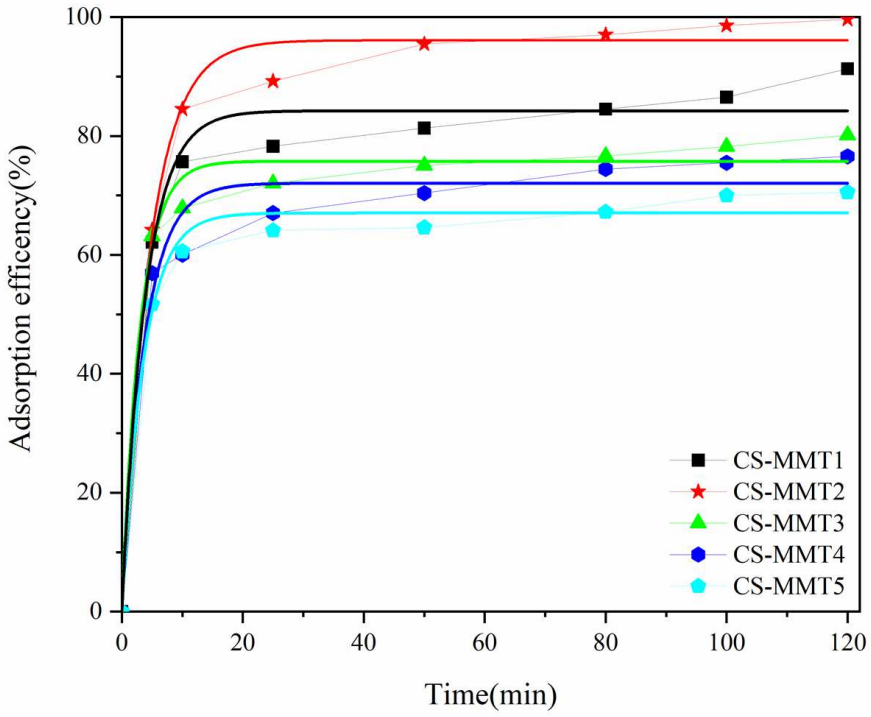

Fig. 5 Adsorption efficiency of CS-MMT composite aerogels for Cu^{2+} at different time

The parameters of the two models are shown in SI Table S2. By comparing the correlation coefficient R^2 of the two models, it is obvious that the pseudo-second-order kinetic equation has a good correlation with the adsorption process. This indicates that the adsorption rate is more related to the number of unoccupied active sites. As the layered space of montmorillonite increases, the porosity increases. This will directly increase the number of active sites and increase the adsorption capacity

220 of Cu^{2+}. Based on the quasi-second-order kinetic equation model, the quasi-second-order rate equation
221 of CS-MMT was shown in Fig. 6. According to the fitting curve of CS-MMTs, the corresponding
222 correlation coefficient R^2 was calculated. The R^2 of CS-MMTs indicates that the adsorption of Cu^{2+} in
223 this system follows a pseudo-second-order kinetic model. CS-MMT2 has the best fit, which can reach
224 0.99937, while Q_e is 9.906 and K_2 is 0.04942.

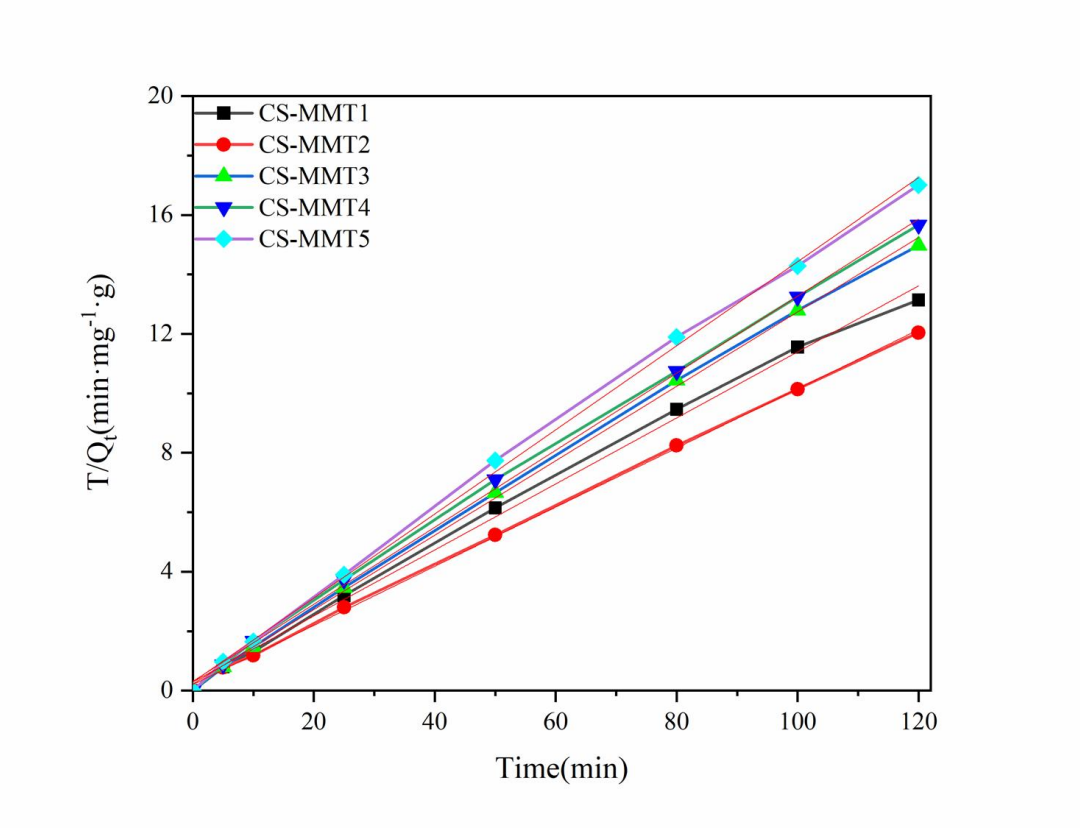

225

226 **Fig. 6** Pseudo-second-order model for adsorption of Cu^{2+} on CS-MMT composite aerogels

227 **Adsorption isotherms and adsorption thermodynamics**

228 As can be seen from Fig. 7, the equilibrium adsorption capacity of the three adsorbents to copper
229 ions increased with the increase of the initial concentration of Cu^{2+} solution until the adsorption was
230 completed. When Cu^{2+} solution is at a low concentration, the adsorption curve rises very fast. When the
231 initial concentration increases to a certain concentration, the increasing rate of adsorbent adsorption
232 gradually slows down, and the curve flattens out to near saturation adsorption.

233 In order to obtain the thermodynamic mechanism of adsorption of Cu^{2+} by CS-MMT composite
234 aerogels at different initial concentrations, the Langmuir equation and Freundlich equation were used
235 to fit the experimental data. The Langmuir isotherm model (Eq. 7) and the Freundlich isotherm model
236 (Eq. 8) are as follows:

237 $$\frac{C_e}{Q_e} = \frac{C_e}{Q_m} + \frac{1}{K_L Q_m} \quad (7)$$

238 $$\ln Q_e = \ln K_F + \frac{1}{n} \ln C_e \quad (8)$$

239 Where Q_e is the adsorption amount of Cu^{2+} per unit mass of adsorbent at the adsorption equilibrium
240 (mg/g) Q_m represents the maximum adsorption capacity of Cu^{2+}(mg/g), and C_e represents the equilibrium
241 concentration of Cu^{2+} after adsorption (mg/L), where K_L and K_F are the adsorption equilibrium constants
242 of Langmuir isotherm equation and Freundlich isotherm equation, and 1/n is the heterogeneity factor.

243 As can be clearly seen in Fig.10, the equilibrium adsorption capacity of the five adsorbents on Cu^{2+}
244 showed a different increasing trend with the increase of the initial concentration of Cu^{2+} solution. When
245 Cu^{2+} is at a low concentration, the adsorption curve rises very fast. When the initial concentration
246 increases to a certain concentration, the increasing rate of adsorbent adsorption volume gradually slows
247 down, and the curve flattens out until it approaches saturation adsorption.

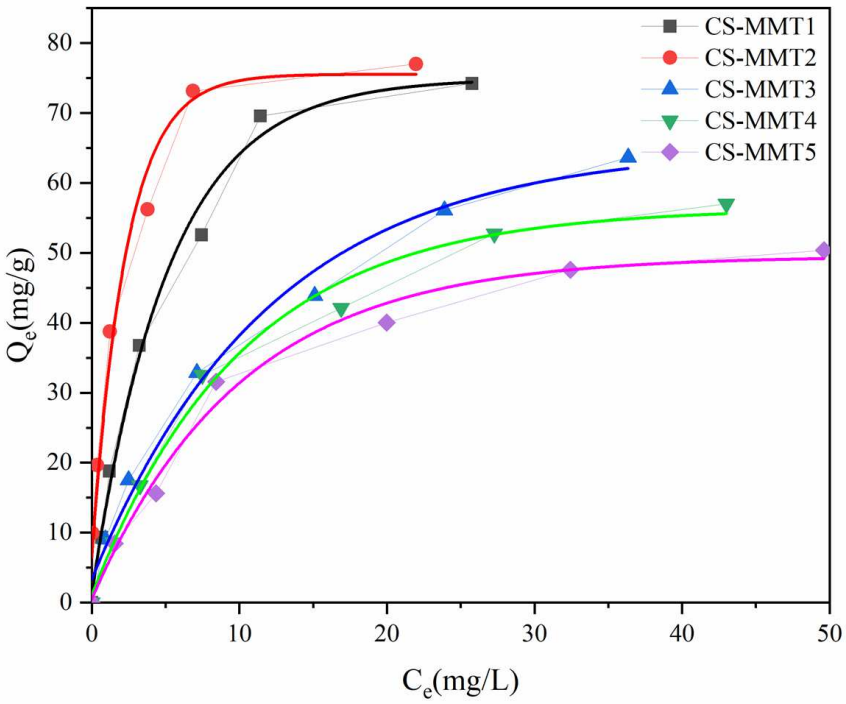

Fig. 7 Adsorption capacity of CS-MMT composite aerogels for Cu^{2+} in different initial solution concentration

The adsorption data were correspondingly fitted to the Langmuir model. The fitting equations of CS-MMTs are shown in Fig.8. The Langmuir and Freundlich parameters for adsorption of Cu^{2+} are sort in SI Table S3, respectively. The maximum adsorption capacity of the CS-MMTs on Cu^{2+} can be estimated according to the Langmuir adsorption model. Under the optimal conditions, the maximum adsorption capacities of CS-MMT composite aerogels for Cu^{2+} were estimated to be 80.38 mg/g, 86.95mg/g, 76.92mg/g, 69.93mg/g, and 60.86mg/g, respectively. Compared with the montmorillonite adsorbent reported in the literature, the CS-MMT2 composite aerogel prepared by this experiment showed quite outstanding adsorption capacity for Cu^{2+} (Table 1). The digital image of the adsorption effect is shown in SI Fig. 4. With the addition of the adsorbent for about 30s, the blue complex will initially form until it becomes stable. After adsorption and centrifugation, the solution was obviously

close to the colorless state.

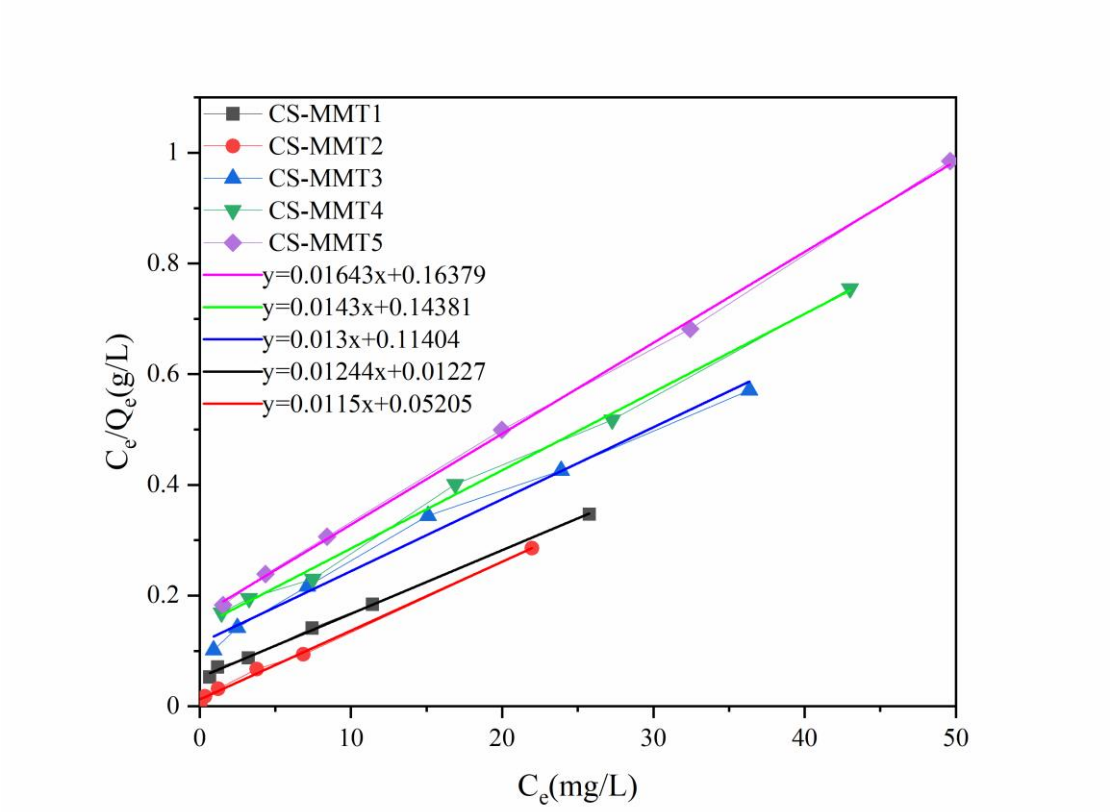

Fig. 8 Langmuir isotherms plots of Cu^{2+} adsorption on CS-MMTs

Table 1 Comparison with other published work

Researchers	**Adsorbent**	**Cu^{2+} Adsorption performance**	**Ref.**
Chen et al.	Fe_3O_4-CS/EDTA	36.52 mg/g	(Chen et al. 2019)
Chu et al.	Arg-Mt	29.15 mg/g	(Chu et al. 2019)

Chu et al.	Histidine modifies montmorillonite	30.72 mg/g	(Chu et al. 2020)
Chu et al.	Montmorillonite was modified by diamino surfactant-containing tetra ammonium cation	29.03 mg/g	(Chu et al. 2020)
Zhang et al.	Magnetic bentonite/carboxymethyl chitosan/sodium alginate hydrogel sphere	56.79 mg/g	(Zhang et al. 2019)
Wu et al.	Magnetic polysaccharide/Go @Fe_3O_4 gel beads	55.96 mg/g	(Wu et al. 2019)
This work	CS-MMT	86.95 mg/g	

265

266 **2.5 The influence of pH on the adsorption effect**

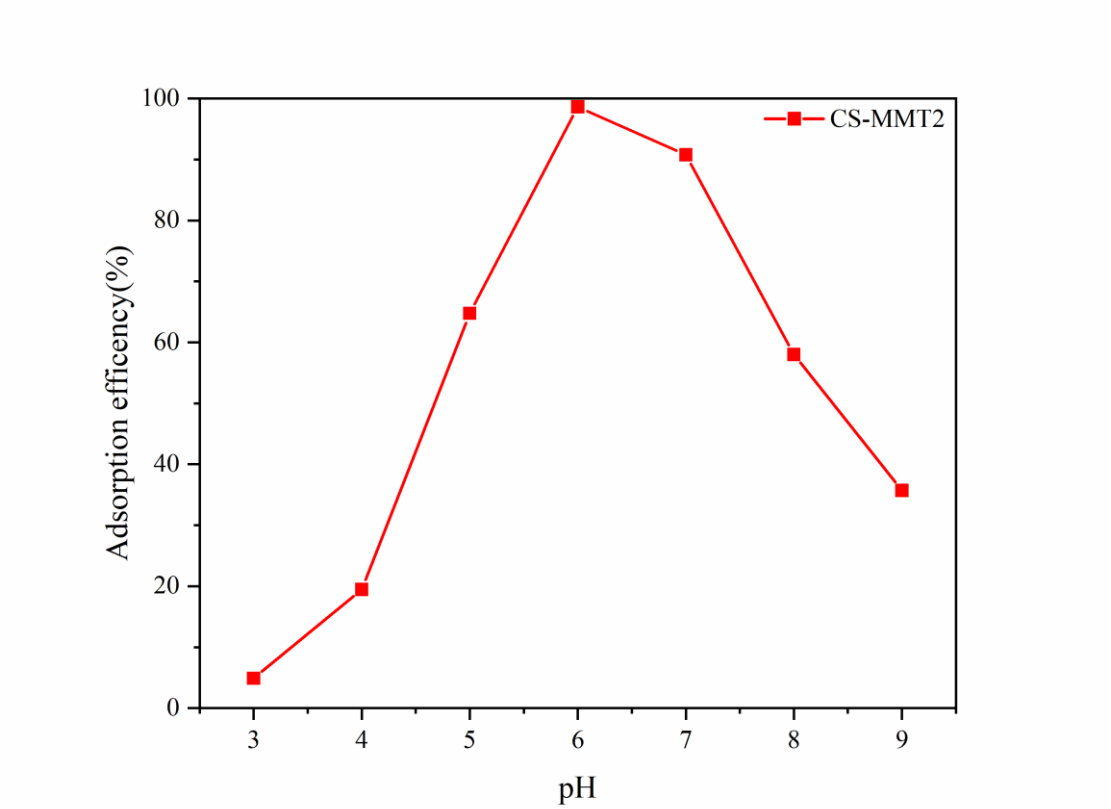

Fig. 9 The effect of solution pH value on the adsorption capacity of Cu^{2+} by CS-MMT2

It can be seen from Fig. 9 that the Cu^{2+} adsorption capacity of CS-MMT2 increases first and then decreases with the increase of the pH of the solution. When the solution is in a low pH range (3.0~4.0), the adsorption effect of CS-MMT2 is limited. This phenomenon can be interpreted as the presence of excess hydrogen ions under a low pH condition, which limits the reaction of chitosan and NH_3 groups. Besides, CS is easy to dissolve in an acidic environment, which is the main reason for the limited adsorption capacity. When the pH value is higher than 4, the adsorption capacity of Cu^{2+} increases significantly. As the pH of the solution increases, the number of hydrogen ions decreases, and protonation increases. There will be more adsorption sites on the surface of CS-MMT2, and the adsorption capacity will also show an increasing trend. At pH = 6, the adsorption capacity reached its peak and then began to decline. Cu^{2+} will form $Cu(OH)_2$ precipitation at higher pH values. This shows from the side that the adsorption capacity of CS-MMT2 for Cu^{2+} decreases. Therefore, pH = 6 is the best service condition for

CS-MMT. Compared with the montmorillonite adsorbent reported in the literature, the CS-MMT composite aerogel prepared in this experiment has a better adsorption capacity for Cu^{2+}.

2.6 Adsorption cycle performance

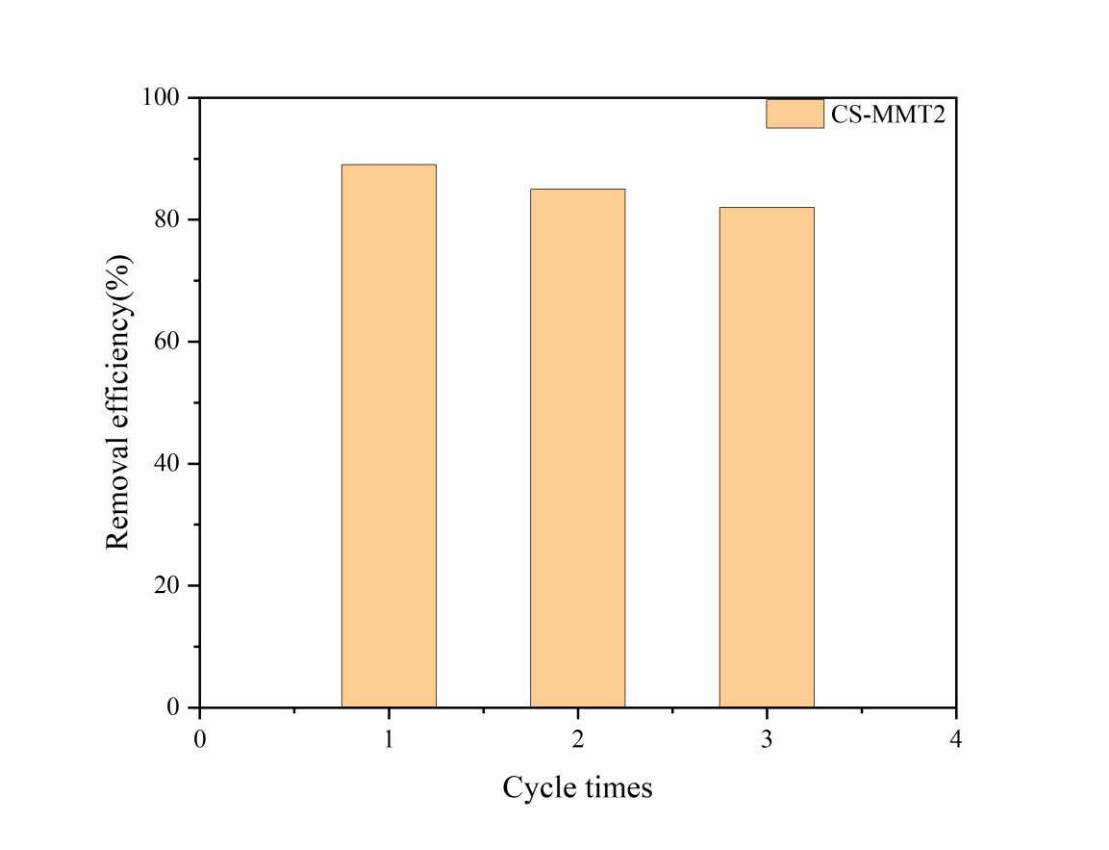

Fig. 10 Circulation capability of CS-MMT2

The regeneration efficiency of adsorbent is an important index to measure the actual use effect of an adsorbent. Generally speaking, effective adsorbent materials not only have high adsorption capacity but also have a great reuse effect. In this cycle experiment, we used a 0.2 mol/L EDTA solution as the desorption solution. The three-cycle effect of CS-MMT2 was measured. The experimental results are shown in Fig. 10. After 3 times of adsorption-desorption, the adsorption efficiency of CS-MMT2 aerogel changed slightly and remained at about 80%. EDTA mainly plays the role of chemically eluting Cu^{2+} in the desorption process and has a certain group repair effect on CS-MMT2. CS-MMT2 aerogel can be regenerated during desorption and incomplete vacuum desorption. But at the same time, certain structural

shrinkage and hole blockage are inevitable. This is due to the massive loss of CS-MMT surface groups during the adsorption and desorption process.

2.7 Discussion on adsorption principle

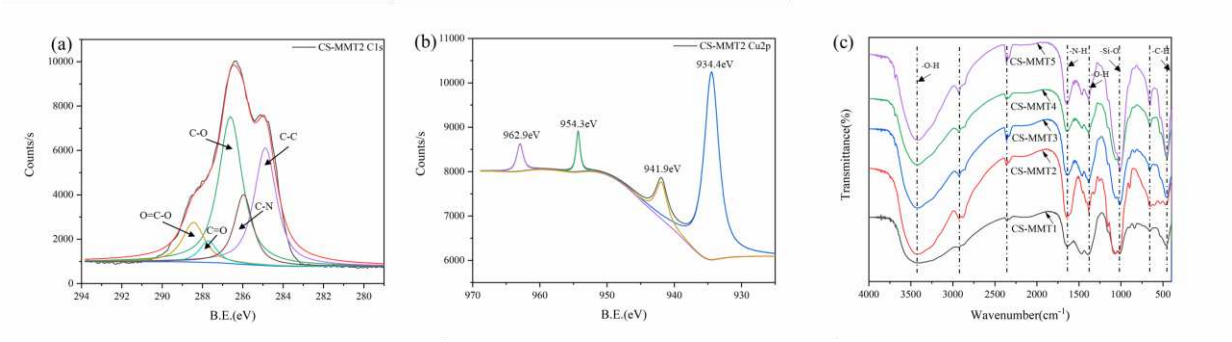

Fig. 11 (a) C1s, (b)Cu2p spin-orbit peaks of CS-MMT2 after adsorption, (c) FT-IR spectra of CS-MMTs after adsorption

To explore the principle of adsorption, we characterized the adsorbed samples. As shown in Fig. 11(a), the C 1s spectra of CS-MMT2 were fitted with three components centered at 284.8, 285.9, 286.6.6, 287.7, and 288.4 eV, which can be assigned to C–C, C-N, C-O, C=O, and O=C-O, respectively. The emergence of a new characteristic peak at 934.4 eV, corresponding to the presence of Cu2p orbital. At the same time, the metal oxidation peak area was changed. Cu^{2+} reacted with the adsorbent to combine part of O. It is the oxygen-containing functional group that participates in the adsorption process. The Cu2p spin-orbit peaks showed that Cu^{2+} replaced the original hydrogen ion to form the corresponding complex. During the adsorption process, C-N, C-O, O=C-O content increased significantly, indicating that Cu^{2+} was successfully adsorbed on CS-MMT2. Therefore, it can be considered that the high adsorption capacity of CS-MMT2 to Cu^{2+} is due to chelating and stacking, and electrostatic attraction. As shown in Fig. 11(c), the intensity of the characteristic peak of the infrared spectrum changed to different degrees after copper ions were adsorbed, which indicats that amino, carboxyl, siloxane, and hydroxyl groups in CS-MMTS were involved in the

312 adsorption of Cu^{2+}.

313 **3. Conclusions**

314 CS-MMT composite aerogels were prepared by freeze-drying adsorption of Cu^{2+}. Montmorillonite
315 has a layered structure. Modifier and physical methods are used to enlarge the distance between the
316 montmorillonite, and CS is grafted on the surface of montmorillonite. The surface contains a large
317 number of active sites, which promote the cross-linking of chitosan and montmorillonite, forming a
318 stable three-dimensional network structure. The experimental results show that CS-MMT2 has good
319 adsorption performance for Cu^{2+}.CS-MMT2 composite aerogel has a highly developed pore structure,
320 high adsorption capacity, fast adsorption and desorption, and can effectively remove Cu^{2+} with
321 remarkable effect. MMT first provides adsorption sites through cation exchange, and the amino group
322 on the surface forms hydrogen bonds with the hydroxyl group of the chitosan, which promotes the
323 cross-linking of the chitosan and montmorillonite in the soil. After 3 times of adsorption-desorption,
324 the removal effect of CS-MMT2 composite aerogel on Cu^{2+} remains about 80%. A feasible method was
325 provided for the selective removal and effective recovery of Cu^{2+} from heavy metal wastewater.

326 **4. Acknowledgment**

327 This work was financially supported by the Key Research and Development Project of Jiangsu
328 Province (BE2019734, BE2017151, BE2016171), the Major Program of Natural Science Fund in
329 Colleges and Universities of Jiangsu Province(15KJA430005), the Program of Science and Technology
330 of Suqian City(M201704, H201801, H201803), the National Natural Science Foundation of China
331 (51702156, 81471183), the Program for Changjiang Scholars and Innovative Research Team in
332 University (IRT_15R35), the Priority Academic Program Development of Jiangsu Higher Education
333 Institutions and the Brand Major Program Development of Jiangsu Higher Education Institutions

(PPZY2015B128). China Scholarship Council under Grant (No. 201908320194), the General Program of Natural Science Fund in Colleges and Universities of Jiangsu Province (19KJB430023), Scientific Research Starting Foundation of Nanjing Tech University, Science and technology innovation project for overseas of Nanjing City, Postdoctoral Science Foundation of Jiangsu Province (2019K005), the High-Performance Computing Center of Nanjing Tech University for supporting the computational resources, China Postdoctoral Science Foundation (2019M661781). Any opinions, findings, and conclusions or recommendations expressed in this paper are those of the authors and do not necessarily reflect the views of these programs.

References

Akar ST, Sayin F, Ozdemir I, Tunc D (2020) A Natural Montmorillonite-Based Magsorbent as an Effective Scavenger for Cadmium Contamination Water Air and Soil Pollution 231 doi:10.1007/s11270-020-04743-3

Baetens R, Jelle BP, Gustavsen A (2011) Aerogel insulation for building applications: A state-of-the-art review Energy and Buildings 43:761-769 doi:10.1016/j.enbuild.2010.12.012

Bailey SE, Olin TJ, Bricka RM, Adrian DD (1999) A review of potentially low-cost sorbents for heavy metals Water Res 33:2469-2479 doi:Doi 10.1016/S0043-1354(98)00475-8

Chen B, Zhao H, Chen S, Long F, Huang B, Yang B, Pan X (2019) A magnetically recyclable chitosan composite adsorbent functionalized with EDTA for simultaneous capture of anionic dye and heavy metals in complex wastewater Chemical Engineering Journal 356:69-80 doi:10.1016/j.cej.2018.08.222

Chu Y, Khan MA, Wang F, Xia M, Lei W, Zhu S (2019) Kinetics and equilibrium isotherms of adsorption of Pb(II) and Cu(II) onto raw and arginine-modified montmorillonite Advanced Powder Technology 30:1067-1078 doi:10.1016/j.apt.2019.03.002

Chu Y, Khan MA, Xia M, Lei W, Wang F, Zhu S, Yan X (2020) Synthesis and micro-mechanistic studies of histidine modified montmorillonite for lead(II) and copper(II) adsorption from wastewater Chemical Engineering Research & Design 157:142-152 doi:10.1016/j.cherd.2020.02.020

Cui S et al. (2018) Preparation of magnetic MnFe2O4-Cellulose aerogel composite and its kinetics and thermodynamics of Cu(II) adsorption Cellulose 25:735-751 doi:10.1007/s10570-017-1598-x

El-Kousy SM, El-Shorbagy HG, Abd El-Ghaffar MA (2020) Chitosan/montmorillonite composites for fast removal of methylene blue from aqueous solutions Mater Chem Phys 254 doi:ARTN 123236

10.1016/j.matchemphys.2020.123236

Fu FL, Wang Q (2011) Removal of heavy metal ions from wastewaters: A review J Environ Manage 92:407-418 doi:10.1016/j.jenvman.2010.11.011

Guo T et al. (2019) Bioinspired self-assembled films of carboxymethyl cellulose-dopamine/montmorillonite Journal of Materials Chemistry A 7:14033-14041 doi:10.1039/c9ta00998a

Hu C, Li GY, Wang YY, Li FY, Guo GG, Hu HQ (2017a) The effect of pH on the bonding of Cu2+ and chitosan-montmorillonite composite Int J Biol Macromol 103:751-757 doi:10.1016/j.ijbiomac.2017.05.065

Hu C, Zhu PF, Cai M, Hu HQ, Fu QL (2017b) Comparative adsorption of Pb(II), Cu(II) and Cd(II) on chitosan saturated montmorillonite: Kinetic, thermodynamic and equilibrium studies Appl Clay Sci 143:320-326 doi:10.1016/j.clay.2017.04.005

Jarup L (2003) Hazards of heavy metal contamination Brit Med Bull 68:167-182 doi:10.1093/bmb/ldg032

Kolpin DW, Furlong ET, Meyer MT, Thurman EM, Zaugg SD, Barber LB, Buxton HT (2002) Pharmaceuticals, hormones, and other organic wastewater contaminants in US streams, 1999-2000: A national reconnaissance Environmental Science & Technology 36:1202-1211 doi:10.1021/es011055j

Li A, Lin RJ, Lin C, He BY, Zheng TT, Lu LB, Cao Y (2016) An environment-friendly and multi-functional absorbent from chitosan for organic pollutants and heavy metal ion Carbohyd Polym 148:272-280 doi:10.1016/j.carbpol.2016.04.070

Liu P, Fan G, Wang J, Zhou G, Cao Y, Han X, Xu X (2020a) Biomimetic mineralization of montmorillonite-based nanomaterials for efficient capture of copper ions Appl Clay Sci 195 doi:10.1016/j.clay.2020.105720

Liu P, Fan GX, Wang JT, Zhou GL, Cao YJ, Han XK, Xu XQ (2020b) Biomimetic mineralization of montmorillonite-based nanomaterials for efficient capture of copper ions Appl Clay Sci 195 doi:ARTN 105720

10.1016/j.clay.2020.105720

Luo P, Zhao YF, Zhang B, Liu JD, Yang Y, Liu JF (2010) Study on the adsorption of Neutral Red from aqueous solution onto halloysite nanotubes Water Res 44:1489-1497 doi:10.1016/j.watres.2009.10.042

Mahouachi L, Rastogi T, Palm W-U, Ghorbel-Abid I, Chehimi DBH, Kuemmerer K (2020) Natural clay as a sorbent to remove pharmaceutical micropollutants from wastewater Chemosphere 258 doi:10.1016/j.chemosphere.2020.127213

Moja TN, Bunekar N, Mishra SB, Tsai TY, Hwang SS, Mishra AK (2020) Melt processing of polypropylene-grafted-maleic anhydride/Chitosan polymer blend functionalized with montmorillonite for the removal of lead ions from aqueous solutions Sci Rep-Uk 10 doi:ARTN 217

10.1038/s41598-019-57079-2

Pierre AC, Pajonk GM (2002) Chemistry of aerogels and their applications Chem Rev 102:4243-4265 doi:10.1021/cr0101306

Qin L et al. (2020) Preparation of ion-imprinted montmorillonite nanosheets/chitosan gel beads for selective recovery of Cu(II) from wastewater Chemosphere 252 doi:ARTN 126560

10.1016/j.chemosphere.2020.126560

Shabbir Z et al. (2020) Copper uptake, essentiality, toxicity, detoxification and risk assessment in soil-plant environment Chemosphere 259 doi:ARTN 127436

10.1016/j.chemosphere.2020.127436

Sun YB, Sun GH, Xu YM, Wang L, Liang XF, Lin DS (2013) Assessment of sepiolite for immobilization of cadmium-contaminated soils Geoderma 193:149-155 doi:10.1016/j.geoderma.2012.07.012

Thit A, Banta GT, Palmqvist A, Selck H (2020) Effects of sediment-associated Cu on Tubifex tubifex - Insights gained by standard ecotoxicological and novel, but simple, bioturbation endpoints Environ Pollut 266 doi:ARTN 115251
10.1016/j.envpol.2020.115251

Uddin MK (2017) A review on the adsorption of heavy metals by clay minerals, with special focus on the past decade Chemical Engineering Journal 308:438-462 doi:10.1016/j.cej.2016.09.029

Wan MW, Kan CC, Rogel BD, Dalida MLP (2010) Adsorption of copper (II) and lead (II) ions from aqueous solution on chitosan-coated sand Carbohyd Polym 80:891-899 doi:10.1016/j.carbpol.2009.12.048

Wang R, Shou D, Lv O, Kong Y, Deng LH, Shen J (2017) pH-Controlled drug delivery with hybrid aerogel of chitosan, carboxymethyl cellulose and graphene oxide as the carrier Int J Biol Macromol 103:248-253 doi:10.1016/j.ijbiomac.2017.05.064

Wu HP et al. (2020) Cetylpyridinium bromide/montmorillonite-graphene oxide composite with good antibacterial activity Biomed Mater 15 doi:ARTN 055002
10.1088/1748-605X/ab8440

Wu HS, Zhang AQ, Wang LS (2004) Immobilization study of biosorption of heavy metal ions onto activated sludge J Environ Sci-China 16:640-645

Wu Z, Deng W, Zhou W, Luo J (2019) Novel magnetic polysaccharide/graphene oxide @Fe3O4 gel beads for adsorbing heavy metal ions Carbohyd Polym 216:119-128 doi:10.1016/j.carbpol.2019.04.020

Yuan P, Tan DY, Annabi-Bergaya F (2015) Properties and applications of halloysite nanotubes: recent research advances and future prospects Appl Clay Sci 112:75-93 doi:10.1016/j.clay.2015.05.001

Zhang H, Omer AM, Hu Z, Yang L-Y, Ji C, Ouyang X-k (2019) Fabrication of magnetic bentonite/carboxymethyl chitosan/sodium alginate hydrogel beads for Cu (II) adsorption Int J Biol Macromol 135:490-500 doi:10.1016/j.ijbiomac.2019.05.185

Zhao Y, Zhong K, Liu W, Cui S, Zhong Y, Jiang S (2020) Preparation and oil adsorption properties of hydrophobic microcrystalline cellulose aerogel Cellulose doi:10.1007/s10570-020-03309-0

Zhu L, Wang L, Xu Y (2017) Chitosan and surfactant co-modified montmorillonite: A multifunctional adsorbent for contaminant removal Appl Clay Sci 146:35-42 doi:10.1016/j.clay.2017.05.027

Zou Y et al. (2016) Environmental Remediation and Application of Nanoscale Zero-Valent Iron and Its Composites for the Removal of Heavy Metal Ions: A Review Environmental Science & Technology 50:7290-7304 doi:10.1021/acs.est.6b01897

Figures

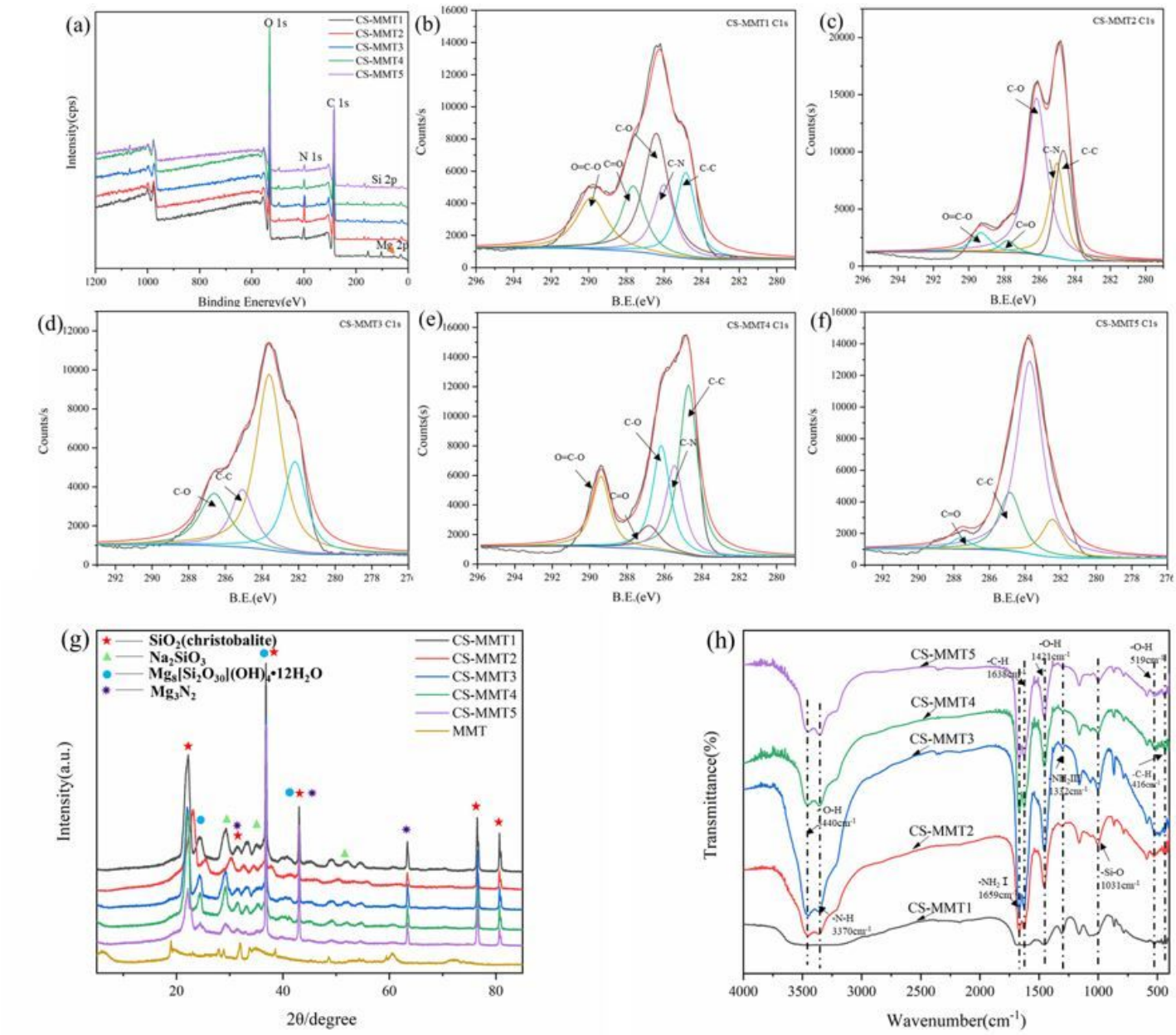

Figure 1

(a) XPS survey spectrum, (b~f) C1s spin-orbit peaks of CS-MMTs, (g) XRD patterns of CS-MMTs and MMT, (h) FTIR spectra of CS-MMTs

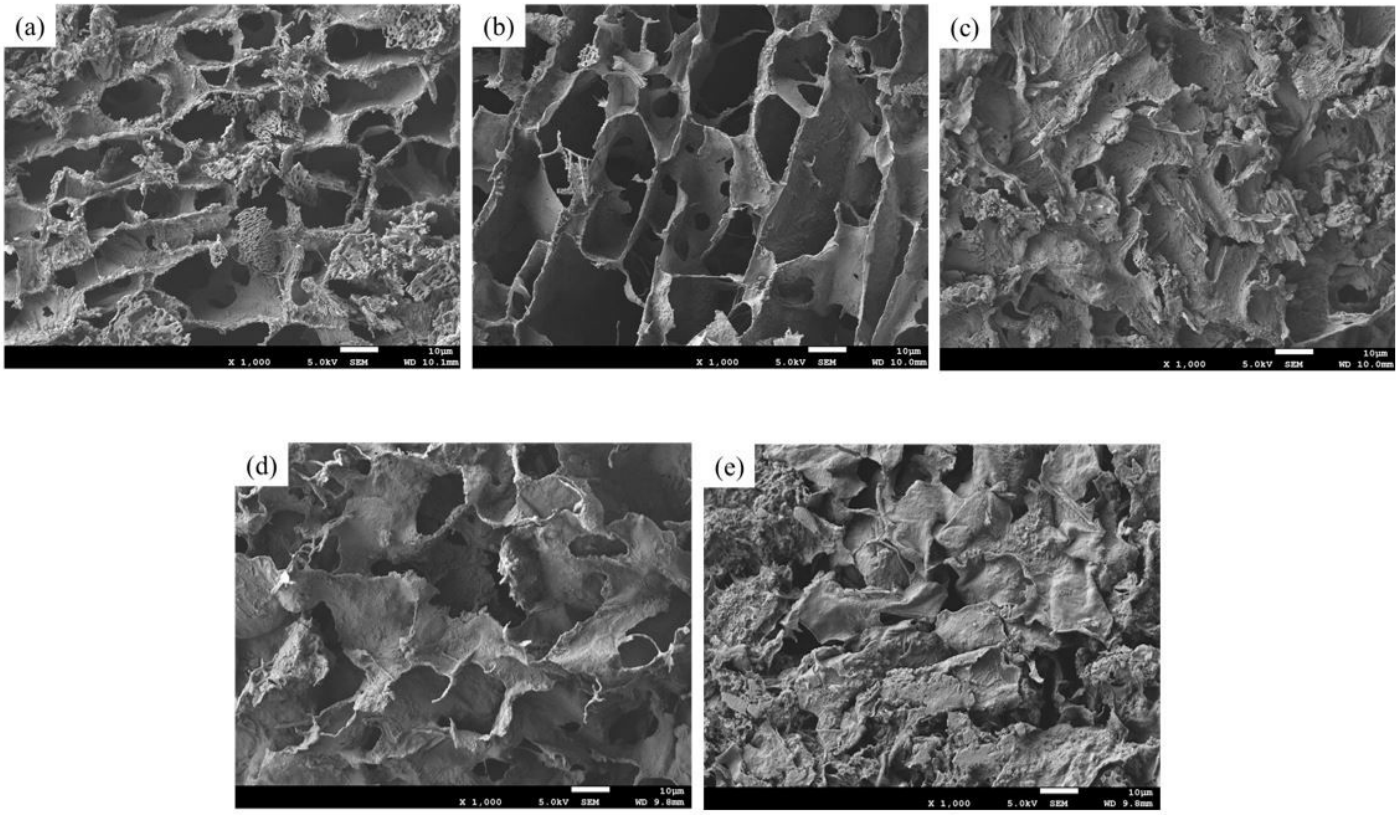

Figure 2

SEM image of (a)CS-MMT1, (b)CS-MMT2, (c)CS-MMT3, (d)CS-MMT4, (e)CS-MMT5

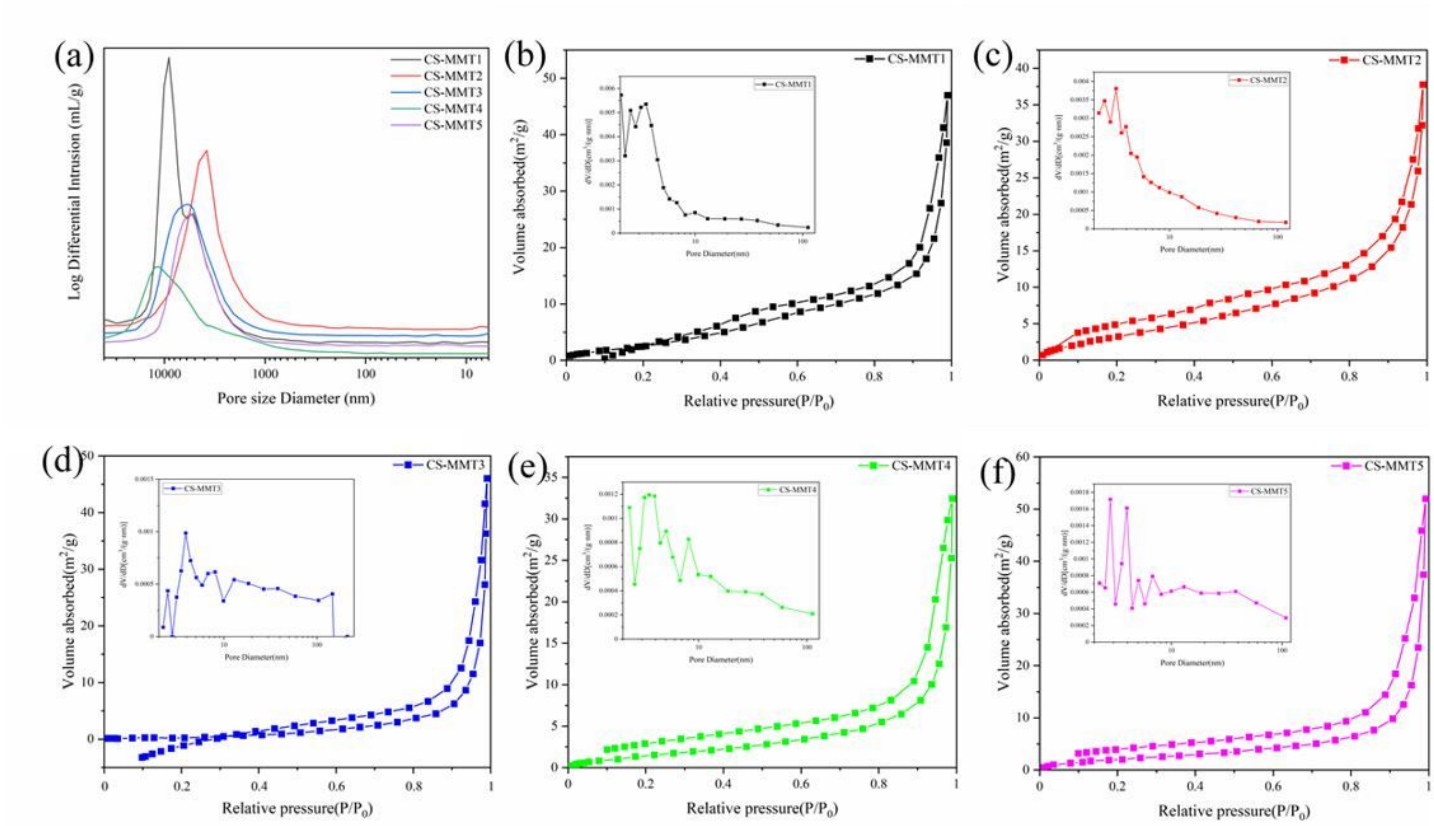

Figure 3

(a) Mercury intrusion test, (b~f) N2 Adsorption–desorption isotherms and pore size distributions of CS-MMT composite aerogels with different components

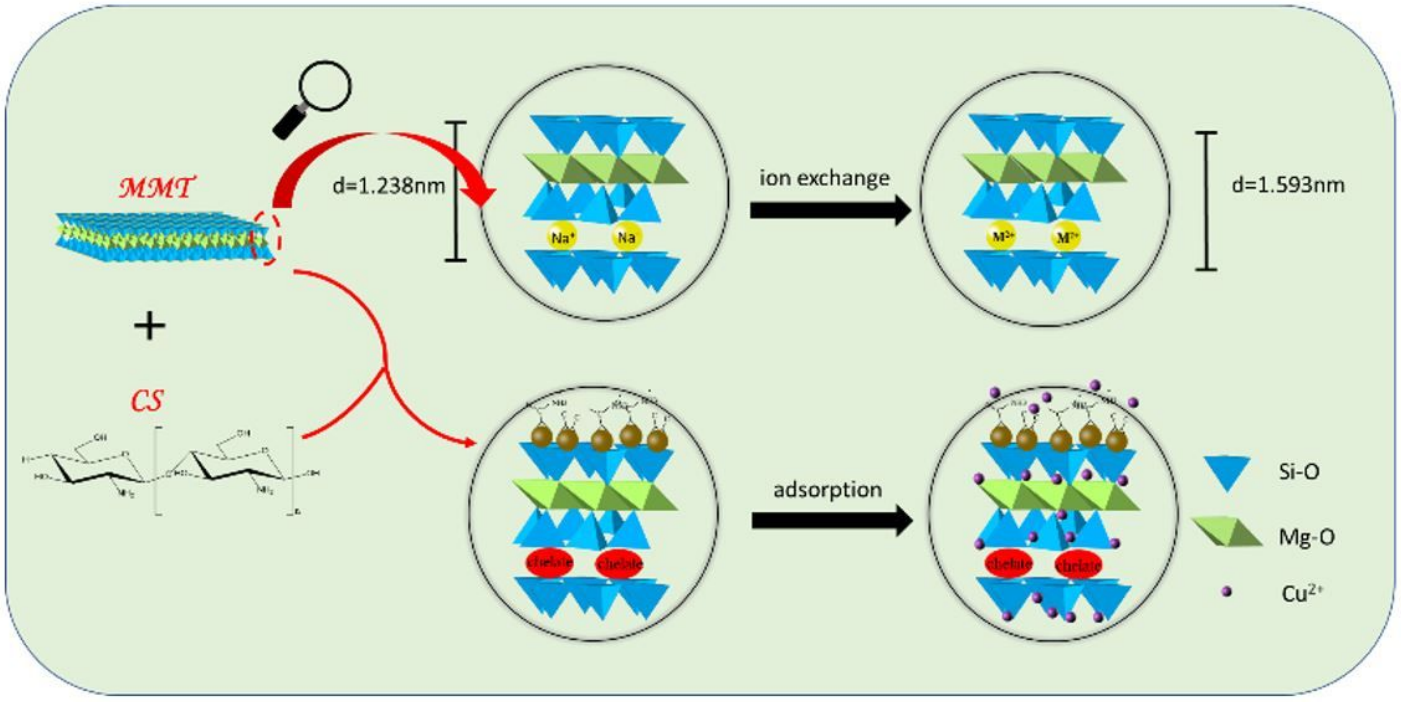

Figure 4

Schematic diagram of structure model and adsorption mechanism

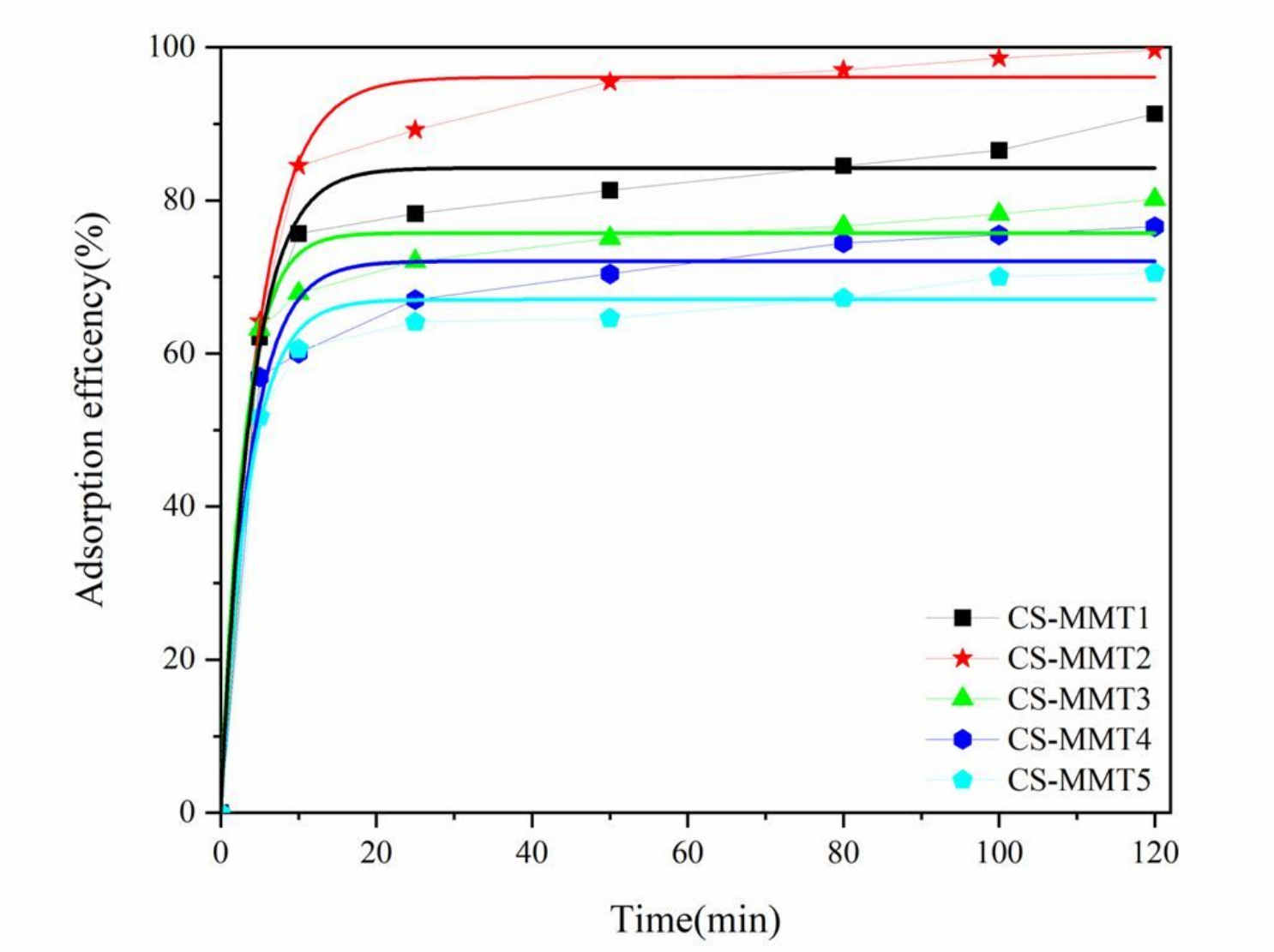

Figure 5

Adsorption efficiency of CS-MMT composite aerogels for Cu2+ at different time

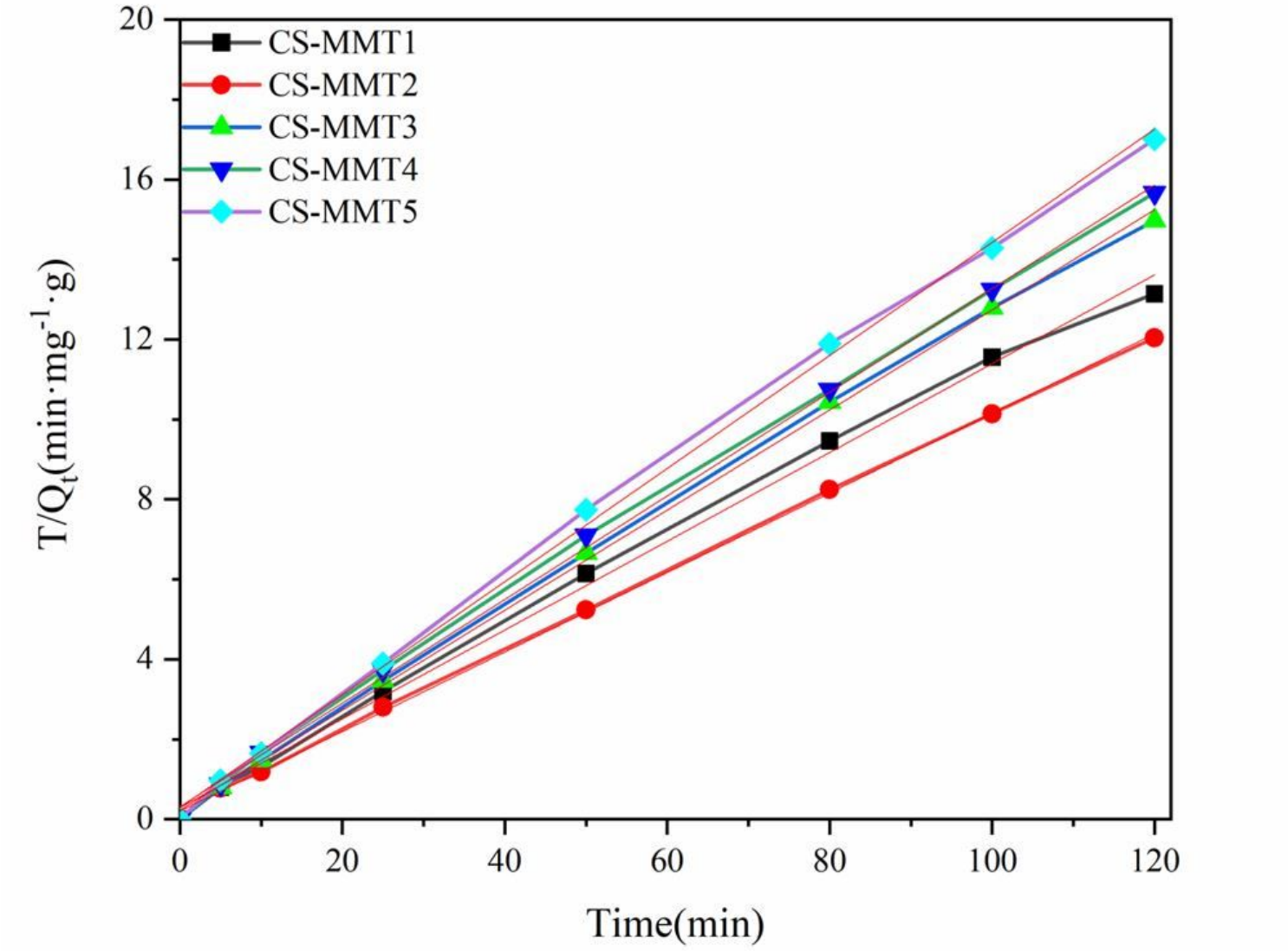

Figure 6

Pseudo-second-order model for adsorption of Cu2+ on CS-MMT composite aerogels

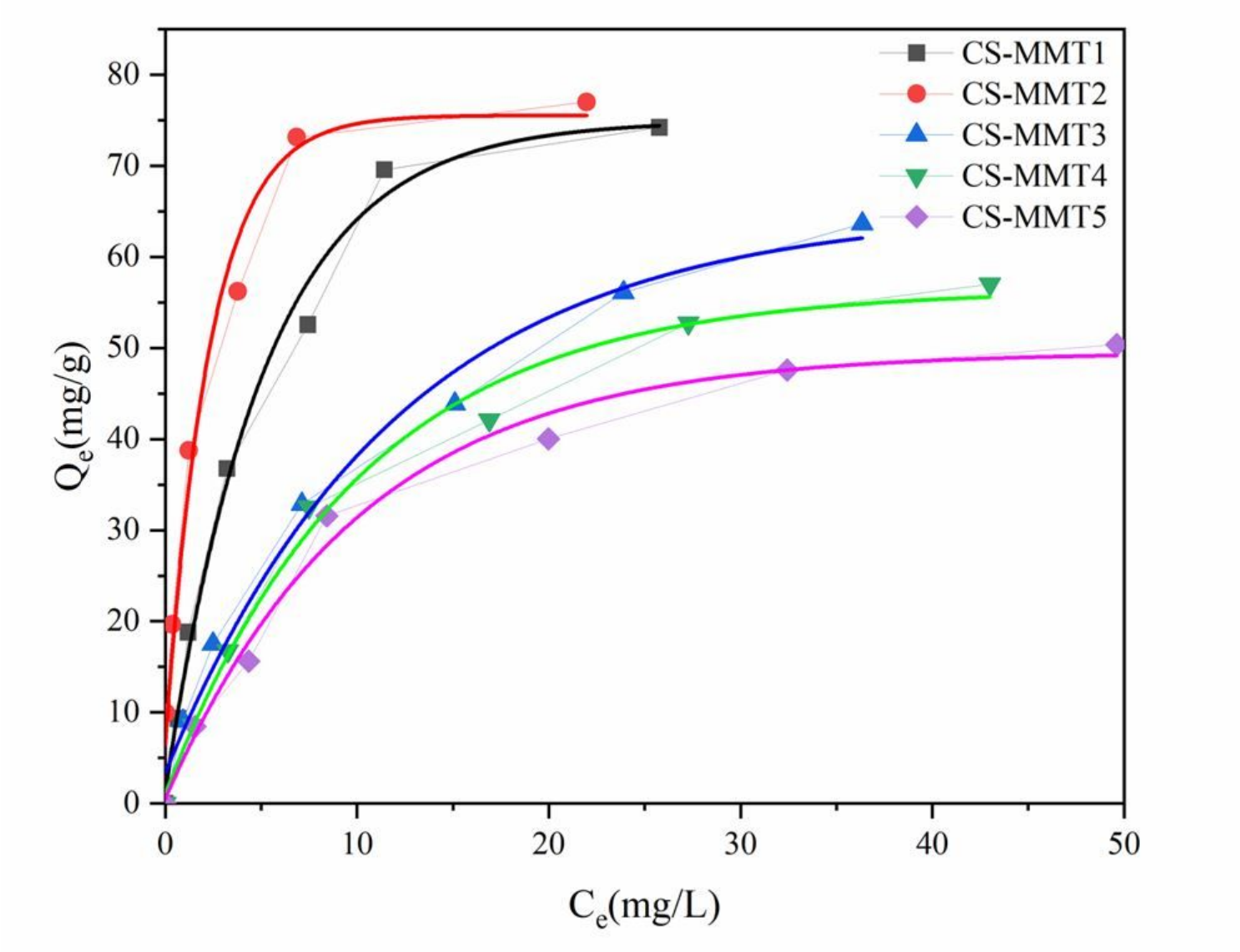

Figure 7

Adsorption capacity of CS-MMT composite aerogels for Cu2+ in different initial solution concentration

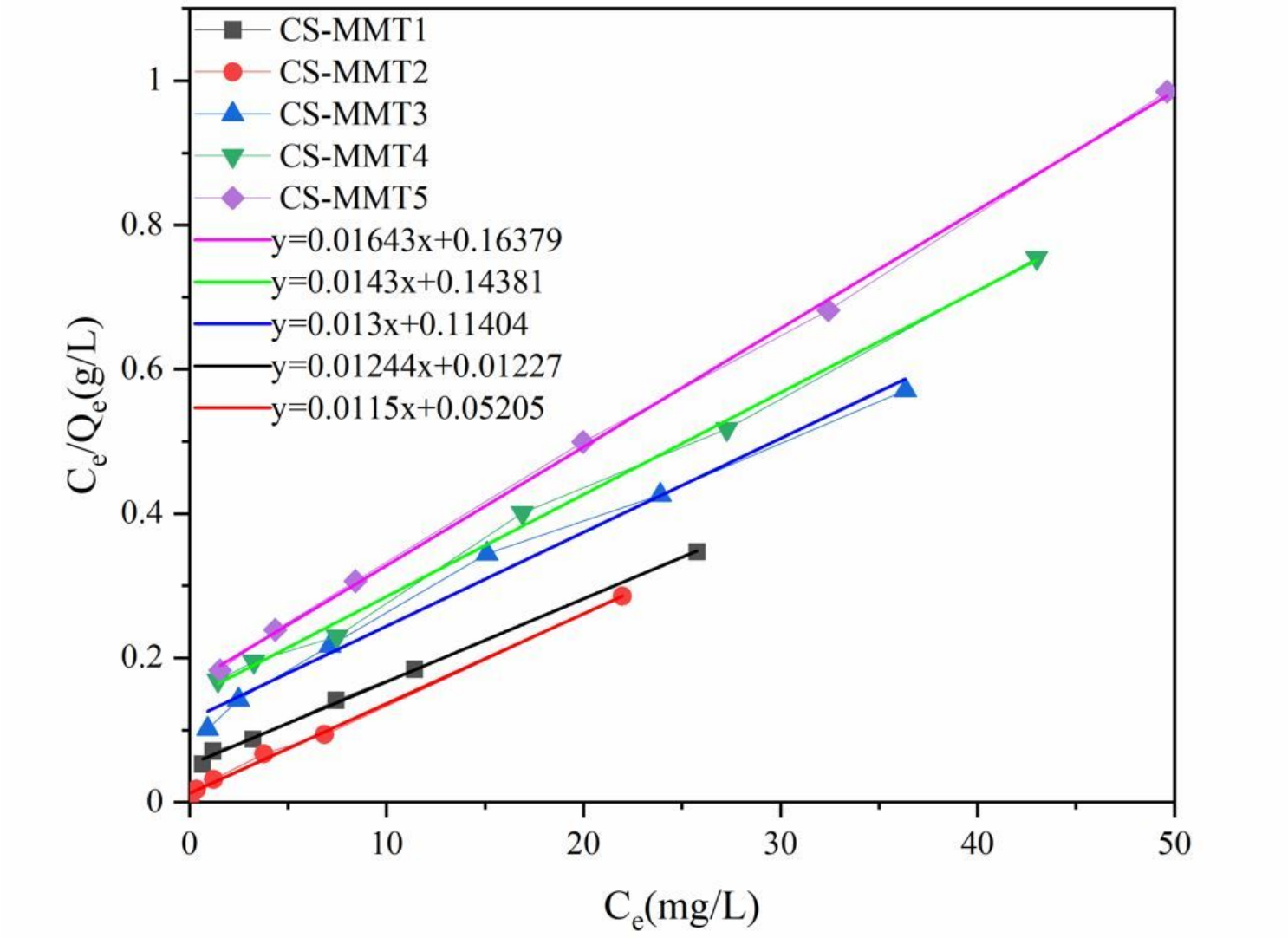

Figure 8

Langmuir isotherms plots of Cu2+ adsorption on CS-MMTs

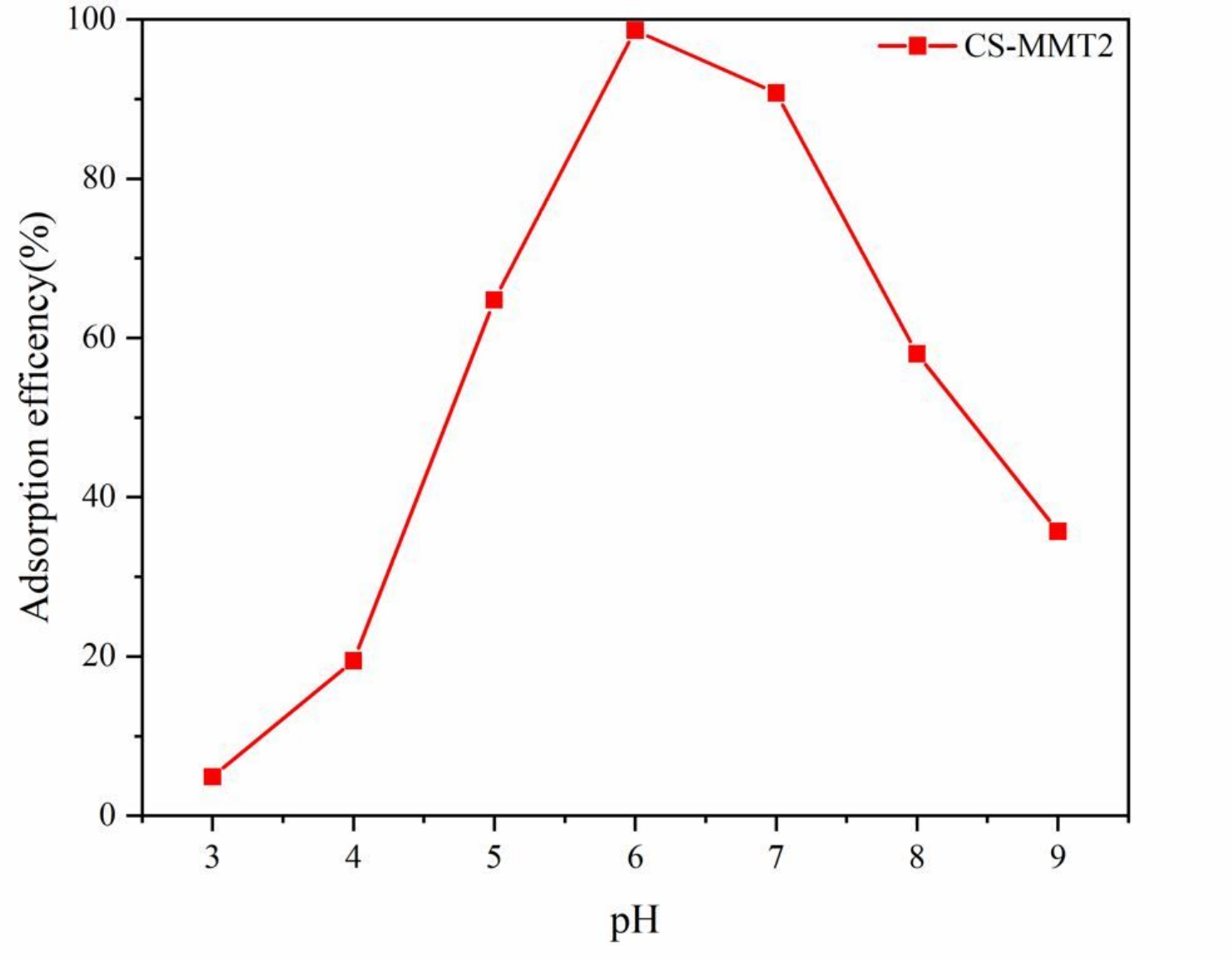

Figure 9

The effect of solution pH value on the adsorption capacity of Cu2+ by CS-MMT2

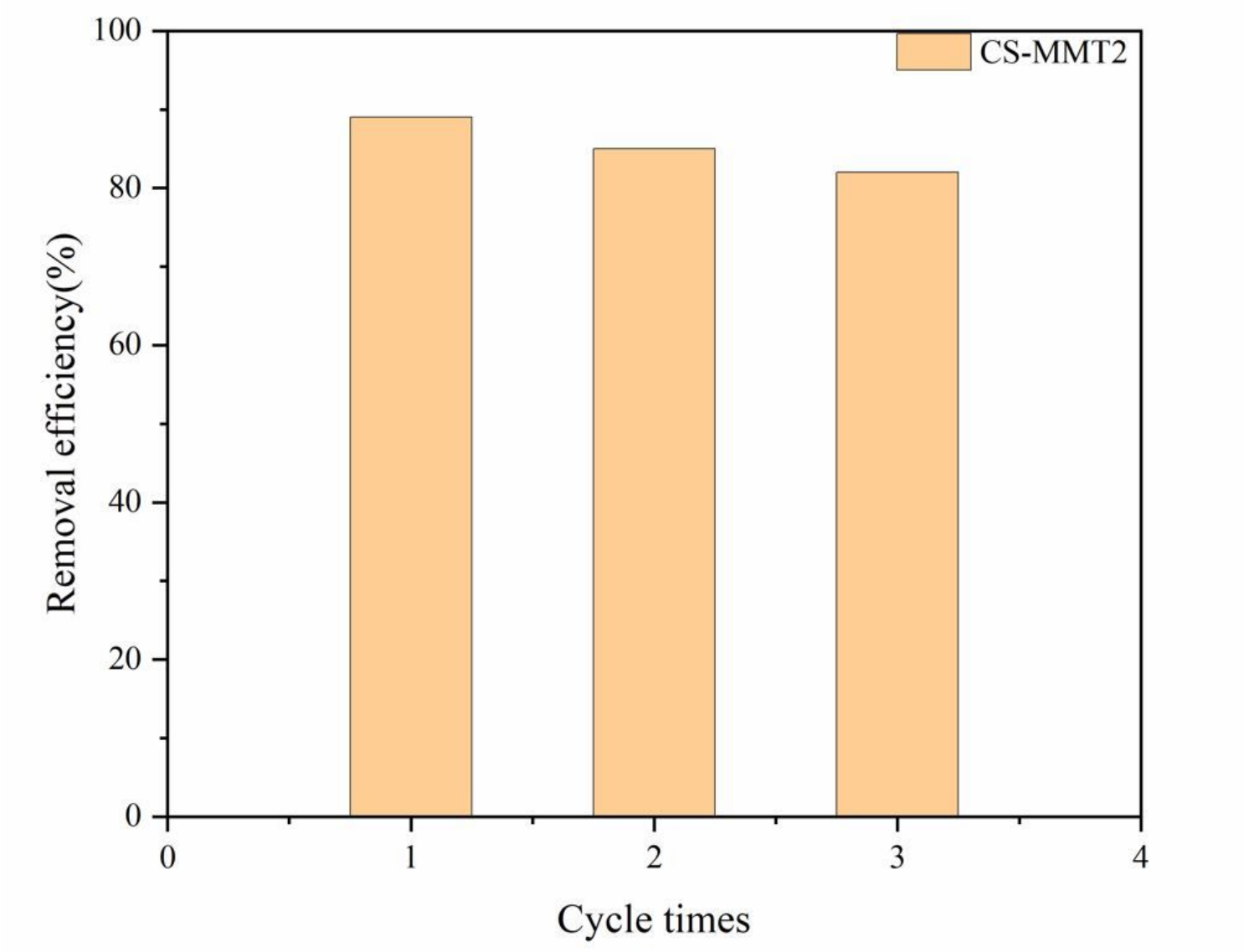

Figure 10

Circulation capability of CS-MMT2

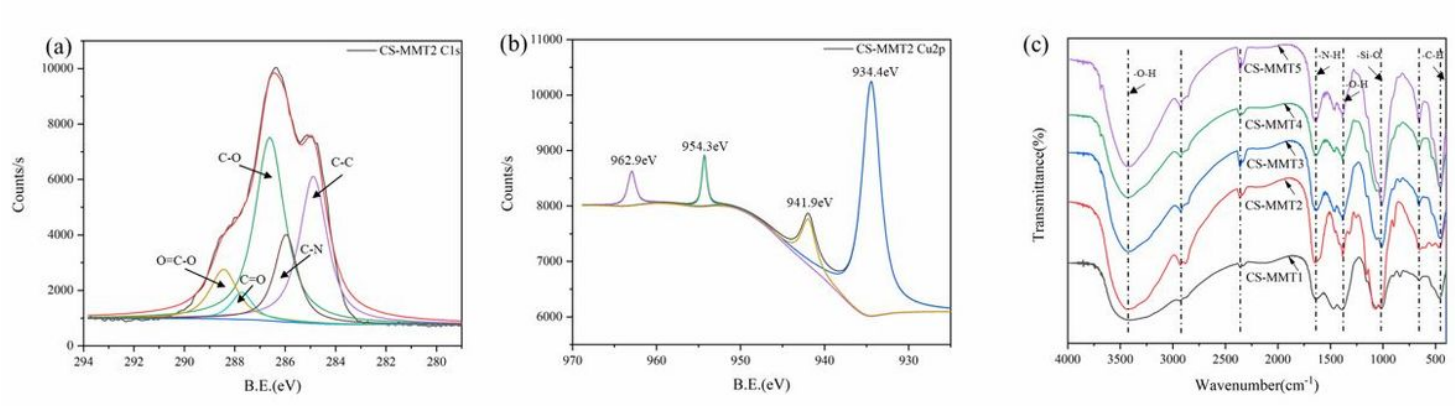

Figure 11

(a) C1s, (b)Cu2p spin-orbit peaks of CS-MMT2 after adsorption, (c) FT-IR spectra of CS-MMTs after adsorption

Supplementary Files

This is a list of supplementary files associated with this preprint. Click to download.

- SI.docx